Nanometer-range atomic order directly recovered from resonant diffuse scattering

M. Kopecký, J. Kub, J. Fábry, and J. Hlinka[*]

Institute of Physics, The Czech Academy of Sciences, Na Slovance 2, 182 21 Prague 8, Czech Republic

The method for three-dimensional imaging with an atomic resolution, based on the measurement of resonant scattering of x rays, is presented and tested on a nanoscale-range occupational ordering of niobium and magnesium ions in the lead magnesium niobate ($PbMg_{1/3}Nb_{2/3}O_3$) single crystal. X-ray diffuse scattering experiments performed at two wavelengths close to the absorption edge of niobium allowed us to record two $1024 \times 1024 \times 1024$ data sets of scattering intensities covering densely a large volume of the reciprocal space (up to $Q_{max} = 8.5 \, \text{Å}^{-1}$, with steps smaller than $\delta Q = 0.05 \, \text{Å}^{-1}$). It is demonstrated that the anomalous part of the scattering intensity, including both discrete diffraction spots and diffuse scattering, can be employed to reconstruct the local atomic environment around the niobium cation up to the distance of several nanometers.

I. INTRODUCTION

Our understanding condensed matter depends largely on structural models based on diffraction experiments. For example, x-ray diffraction exploits the fact that the electron density in the real space is related to the amplitudes and phases of scattered waves in the reciprocal space through the Fourier transform. Still, most experiments provide only the information on the scattering amplitudes, and the phases must be deduced.

The standard approaches to the phase problem are well known [1–3]. For example, structures of monoatomic crystals and liquids or of other simple systems can be often resolved directly from the atomic pair-distribution function, given by the Fourier transform of the scattering intensity only (the Patterson function [1,4,5]). The missing information about the phases is obviously compensated by our *a priori* knowledge of such structures. Structural models of more complex but periodic or quasiperiodic crystal structures [6,7] are largely restricted by the crystallographic space group symmetry and, if needed, the phases of the scattered waves can be efficiently explored for instance by the charge flipping algorithm [8]. However, all these approaches become much less convenient when addressing structures with many degrees of freedom, such as partially disordered crystals [9,10] or crystals of biological molecules [11].

An alternative strategy is to learn about the phases of the scattered waves directly from the experiment. The most common method, EXAFS (extended absorption fine structure [12,13]), exploits the wavelike nature of photoelectrons ejected from the absorbing atom. The forward-propagating electron waves interfere with the electron waves scattered backward from the surrounding atoms and the relative phases of these interfering waves depend on the interatomic distances. In this way, one can probe the radial distribution of the electron density of the few nearest neighbors of the absorbing atoms. Another method is x-ray fluorescence holography with atomic resolution [14,15]. In this case, the atoms of a selected element, excited by a suitable ionizing beam, are emitting fluorescence photons. The undisturbed portion of the fluorescence wave (the holographic reference wave) interferes with the waves scattered on the surrounding atoms (the object wave). The relative phases between the reference wave and the object wave depend on the direction of scattering and on the positions of surrounding atoms. Angular dependence of this interference pattern constitutes a hologram which can be used for a three-dimensional reconstruction of the surroundings of atoms of a selected element. Unfortunately, because of the fast decay of the spherical reference wave with the increasing distance, the x-ray fluorescence holography also provides access to the shortest distances only.

Here we report a method allowing us to reconstruct directly the structure at longer distances as well. We exploit the fact that the *resonant (anomalous) component of the diffuse scattering* has a well-defined phase shift with respect to the classical, nonresonant part [10]. Let us consider a set of atoms in positions $\mathbf{r}_j, j \in S$. Provided that a subset of resonantly scattering atoms at $\mathbf{r}_i, i \in A \subset S$ belongs to the same element, the resonant diffuse scattering intensity I_a at the scattering vector $\mathbf{Q} = \mathbf{k}_{inc} - \mathbf{k}_{fin}$ can be expressed as [16,17]

$$I_a(\mathbf{Q}) \propto 2\text{Re}\left(\Delta f_{res}^* \sum_{j \in S} \sum_{k \in A} f_j(\mathbf{Q}) e^{-i\mathbf{Q}.(\mathbf{r}_j - \mathbf{r}_k)} \right), \quad (1)$$

where f_j is the atomic scattering factor of atom j multiplied by the corresponding Debye-Waller factor, Δf_{res} is the resonant part of the atomic scattering factor common to atoms from the set A, and $\mathbf{k}_{inc}, \mathbf{k}_{fin}$ are the wave vectors of the incident and the scattered wave, respectively. In practice, $I_a(\mathbf{Q})$ can be obtained as a difference between the scattering intensities detected at two very close incident x-ray photon energies [16,17]. The essential principle of the method relies on the fact that the phase factor $e^{-i\mathbf{Q}.(\mathbf{r}_j - \mathbf{r}_k)}$ is determined by the relative position of an atom j with respect to the positions of the resonant scatterers. Consequently, resonant scattering bears complete information about the surroundings of resonant scatterers. More precisely, $f(\mathbf{r}) \propto \int I_a \exp(i\mathbf{Q} \cdot \mathbf{r})$ (real-space reconstructed image) is a weighted pair-distribution function, where all the pairs contain at least one atom of a selected resonant element. The function $f(\mathbf{r})$ can be thus normalized as the averaged electron density *around the resonantly scattering atom*.

The aim of this work is to demonstrate that the proposed method allows us to image the nanometer-range correlations in the Nb/Mg occupational distribution in a cubic perovskite

---

*hlinka@fzu.cz

$PbMg_{1/3}Nb_{2/3}O_3$ (PMN) [18–20]. PMN is probably the most enigmatic example of a relaxor material [18–25]. In spite of keeping its $Pm\bar{3}m$ ($Z = 1$) average cubic structure in the entire temperature range, it shows a high permittivity and an extraordinary glasslike dielectric behavior indicating a very broad range of relaxational frequencies in the system [20,26–29]. The origin of the glasslike dielectric behavior is often related to the random electric fields associated with the frustrated occupational ordering on the ABO_3 perovskite B site [20,30–32]. Recently, lot of effort is spent on computer simulations of the structural and dielectric properties of relaxors within rather sophisticated atomistic models [33–40]. Disordered B-site distribution is considered as a key ingredient there. Thus, detailed experimental studies of the Nb/Mg distribution are highly needed.

The current picture of the B-site ordering in PMN mostly relies on the observed diffuse diffraction spots with half-integer indices ($h + 1/2$, $k + 1/2$, $l + 1/2$) of the reciprocal lattice of the average perovskite structure, suggesting a rocksalt (checkerboard) ordering in domains of about 5 nm diameter [41–44]. Originally, this short-range coherency used to be explained by the incompatibility of the 2:1 stoichiometric Nb:Mg ratio with a simple rocksalt order, but later it was realized that one B-site sublattice of the ordered region could be disordered itself in a way that overall stoichiometry and charge balance is preserved [45,46]. Intensity contrast variations at 2–6 nm scale were also clearly identified in several transmission electron microscopy studies [47–50], even though the direct interpretation of these images is also far from being obvious [32,51]. Moreover, the investigations of solid solutions of PMN and related materials suggest that the nature of the chemical short-range order within the disordered sublattice of PMN could be more important for the relaxor properties than the presence and the size of ordered regions themselves [46]. Nevertheless, as far as we know, no three-dimensional (3D) picture of the short-range occupational correlations was available so far.

II. EXPERIMENT

The x-ray scattering intensity used in the present work was measured at the synchrotron facility in Trieste, Italy. The PMN sample, cut from a similar crystal as used in Refs. [52,53], polished to a 50 μm thick plate with the surface parallel to the (111) crystallographic plane, was illuminated by a monochromatic beam with the cross section of 0.3×0.3 mm^2. The intensity patterns were recorded in the transmission mode using a large area detector Pilatus 2M positioned at the distance of 85 mm behind the sample. The energy threshold of the detector was set to 15 keV in order to cut off the fluorescence photons emitted by Pb atoms. The reciprocal space was scanned by rotating the sample around the axis perpendicular to the incident beam in the angular range of $\pm60°$, which was quite sufficient owing to the sample symmetry. The sample was moving during each exposure by $0.2°$, which corresponded to the step between the consequent frames. The acquisition time of 10 s per frame resulted in smooth diffuse scattering patterns. Additional frames with acquisition time of 1 s and with a set of aluminum absorbers of total thickness of 3.7 mm placed in the primary beam

were collected in order to measure intensities of the strong diffraction peaks without saturation of the detector.

Overall, collected scattering intensities covered densely a large volume of the reciprocal space (up to $Q_{max} = 8.5 \text{ Å}^{-1}$, with steps smaller than $\delta Q = 0.05 \text{ Å}^{-1}$). Two data sets at photon energies of $E_1 = 18.971$ keV and $E_2 = 18.500$ keV were collected. The energy E_1 was chosen just below the niobium K absorption edge (18.986 keV) in order to get a strong resonant component in the scattering from the niobium atoms. The data acquired at the energy E_2 far from the absorption edge were used as the reference data with a small portion of the resonant scattering [11,17]. The experimental data were corrected for the beam polarization, the scattering in air, detector efficiency, instrumental resolution, and absorption in the sample. Individual frames were merged and transformed to the regular grid in the reciprocal space resulting in three-dimensional intensity maps, each of them stored in the matrix of $1024 \times 1024 \times 1024$ points. The intensity maps collected at the photon energies E_1 and E_2 were subtracted obtaining thus a three-dimensional map of the anomalous part of the x-ray scattering intensity.

The present data were taken at ambient conditions. Since the experiment has been carried with a 50 μm thick sample in a transmission mode and both large surfaces of the sample were carefully polished to the optical quality, the surface layer effects can be neglected. Moreover, the absence of the surface effects was also reconfirmed visually by comparison with the reference diffuse scattering data selected and displayed in Ref. [54].

The major part of the background in the scattering patterns is constituted by fluorescence from the lead ions excited at photon energies E_1 and E_2 higher than the L absorption edge of Pb. However, the energy of these fluorescence photons lies far below the energy threshold set on the Pilatus 2M detector and the detector electronics are able to reject the registration of the fluorescence photons. The scattering in air was reduced using the system of four slits and a collimator in front of the sample. In spite of this strong reduction of unwanted signal, the background of the order of 10% is still present in the raw data. For this reason, further background reduction was done numerically during the data processing together with the correction for absorption in the sample in order to eliminate the contribution of background to the anomalous scattering patterns. The presence of strong slowly varying background in the experimental data is related by the Fourier transform to an artifact in the real-space image located in the vicinity of the origin of coordinates. However, the quality of the real-space image indicates the absence of strong background in the processed data. In any case, residual background in the reciprocal space has no influence on the peak-to-valley values of the electron density in the reconstructed real-space image.

III. RESULTS

A typical x-ray diffuse scattering pattern at a planar cross section through the reciprocal space away from the diffraction peaks is shown in Fig. 1(a). Most of the observed intensity is due to the well-known displacive disorder of Pb ions [55], which results in characteristic diffuse streaks, running through the Bragg peak positions along ⟨110⟩ directions [54,56–61],
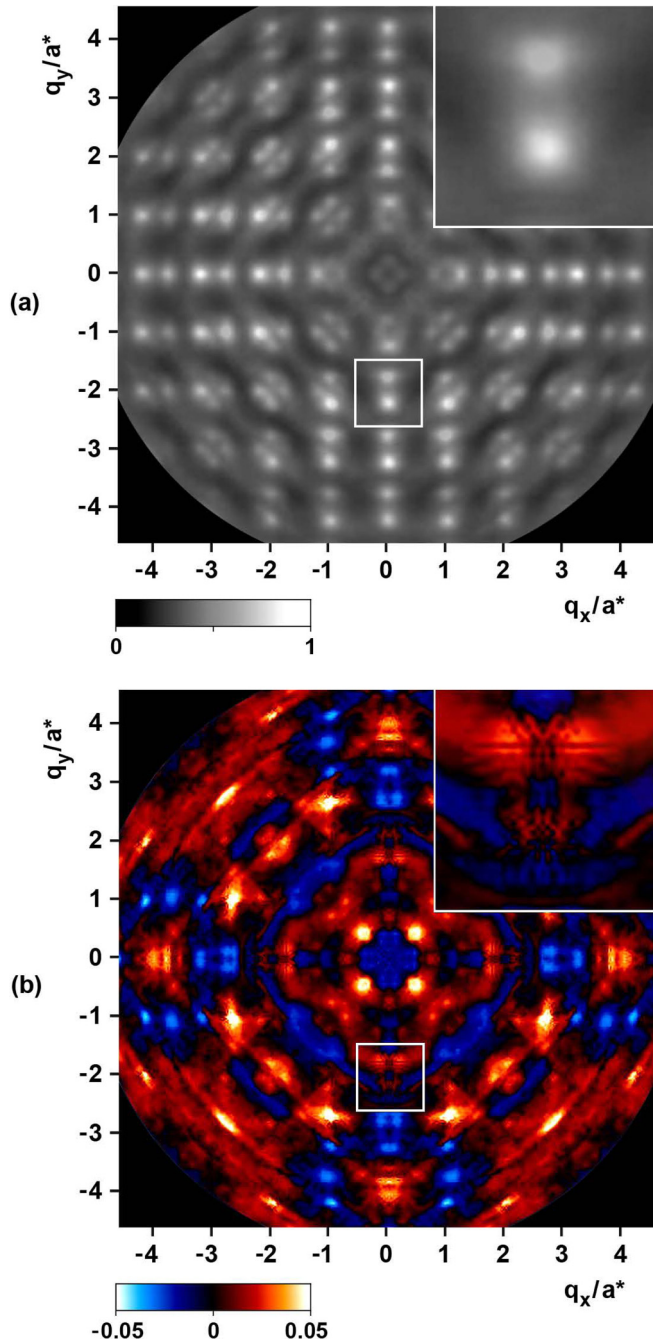
FIG. 1. The intensity map of x-ray diffuse scattering from the PMN single crystal in the $(0\ 0\ 0.25a^*)$ plane of the reciprocal space. (a) Data collected at the photon energy of 18.500 keV. (b) The anomalous portion of the x-ray diffuse scattering obtained as difference between the data taken at the photon energies of 18.500 keV and 18.971 keV. The insets show the enlarged part of the scattering intensity from the marked regions, $a^* = 2\pi/a$ refers to the lattice parameter of PMN ($a = 0.405$ nm).

and which is often interpreted in terms of polar nanoregions [18,22,23,55,58,62]. For example, the two bright spots enlarged in the inset to Fig. 1(a) are due to these diffuse streaks. Figure 1(b) depicts the anomalous portion of the x-ray scattering intensity in the same reciprocal plane. The scale of Fig. 1(b) includes positive as well as negative values.

The sign contains information on the phase of the scattered waves. Here the above mentioned diffuse streaks due to the displacive disorder of Pb ions are largely absent. This is in agreement with expectations that the resonant scattering pattern shows structural information related to the positions of niobium ions. In addition, the resonant scattering patterns have a richer structure [see the inset in Fig. 1(b)]. The accurate determination of this fine structure is essential for the feasibility of the direct reconstruction of the electron density function $f(\mathbf{r})$ by the Fourier transform.

Obviously the most relevant information about the correlations in the occupation of the perovskite B sites is encoded in the intensities and the shapes of the diffuse spots near the reciprocal points with half-integer indices ($h + 1/2$, $k + 1/2$, $l + 1/2$). For example, these spots can be seen in the ($hk2.5$) reciprocal plane displayed in Fig. 2 (the spots located at the corners of the enlarged insets). As expected, these spots are much more dominant in the anomalous part of the scattering [Fig. 2(b)].

The measured three-dimensional pattern of resonant scattering, including both the diffraction peaks and x-ray diffuse scattering was used to reconstruct a three-dimensional real-space image of the electron density around the niobium ion. The electron density variations at B sites are highlighted in Fig. 3. The color of the symbols in Figs. 3(a) and 3(b) varies because the averaged electron density at various B sites around the fixed niobium ion is varying. These variations show systematic short-range correlations in the occupation of the perovskite B sites by niobium and magnesium ions. This is apparent by direct inspection of the values of $f(\mathbf{r})$ at B-site positions, $f_B = f_{[i_x,i_y,i_z]} = f(ai_x\mathbf{x}_0 + ai_y\mathbf{y}_0 + ai_z\mathbf{z}_0)$, where $\mathbf{x}_0, \mathbf{y}_0, \mathbf{z}_0$ are the Cartesian unit vectors, a is the lattice parameter, and i_x, i_y, i_z are integers. The sites with the $i_x + i_y + i_z$ sum equal to even number have visibly higher electronic densities than the neighboring sites with $i_x + i_y + i_z$ odd. Clearly this testifies the anticipated 3D checkerboard oscillations of the niobium occupational probability. These oscillations are apparent up to 3 nm distance from the given niobium ion.

For a more quantitative description of the B-site occupational correlations, we have compared the individual values f_B in the imaged 3D area with the average value $\widehat{f}_B$, obtained from the Fourier transform of the Bragg reflections of the average $Pm\bar{3}m$ structure. Absolute values of the relative density deviations $\delta_B = (f_B - \widehat{f}_B)/\widehat{f}_B$ at a given B site are plotted in Fig. 4 as a function of the interatomic distance. Among others, this plot contains data corresponding to the correlations between B sites located in the direction of the body diagonal, the face diagonal, and the edge of the reference cubic unit cell, respectively. Within the precision of our experiment, all these data fall on a single master curve, allowing us to conclude that the B-site occupational correlations are largely isotropic. The initial slope of the master curve can be fit to $0.32 \exp(-|\mathbf{r}|/\xi)$ with $\xi = 1.41a$ but the entire region is much better adjusted to a sum of two exponentials $c_1 \exp(-|\mathbf{r}|/\xi_1) + c_2 \exp(-|\mathbf{r}|/\xi_2)$ with $c_1 = 0.258$, $c_2 = 0.032$, $\xi_1 = 1.22a$, $\xi_2 = 3.51a$. Interestingly, the leading correlation length is in both cases less than 0.6 nm (or 1.5 unit cells). It suggests that B-site distribution in PMN is mostly determined by the short-range correlations (discussed, e.g., in Ref. [63]). Let us emphasize that this correlation length
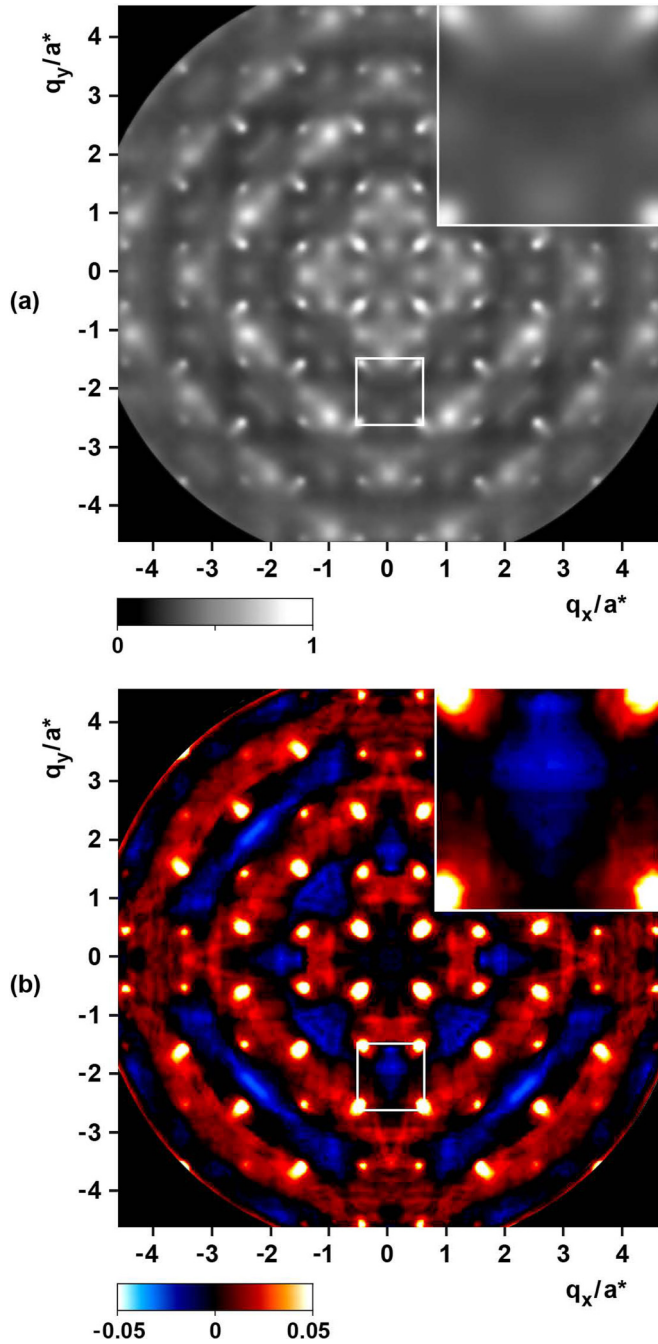
FIG. 2. The intensity map of x-ray diffuse scattering in the $(0\ 0\ 2.5a^*)$ plane of the reciprocal space collected at the photon energy of 18.500 keV (a) and the anomalous portion of it obtained as difference between the data taken at the photon energies of 18.500 and 18.971 keV (b).

FIG. 3. The real-space image of the average surroundings of niobium ions reconstructed from the measured $I_a(\mathbf{Q})$. The coordinate system is related to the reference niobium ion at $\mathbf{r} = (0,0,0)$. Top (a), the reconstructed 3D image. For clarity, lead and oxygen ions are suppressed. Middle (b), the atomic plane parallel to the (001) crystallographic plane at $z = 0$. Bottom (c), reconstructed average electron density function $f(\mathbf{r})$ along the (100) direction. The horizontal line in (c) stands for the average B-site electron density $\widehat{f}_B \doteq 34\ e\,\text{Å}^{-3}$ obtained from the Bragg reflections only. Left side of (c) gives the color code for the data displayed in (a) and (b).

differs from the Scherrer formula length evaluated from the width of the diffuse superstructure scattering peaks detected in the standard diffraction experiments [42,64]. In either case, the correlation function of Fig. 4 may serve as a model-free reference result for any realistic model of the B-site atomic distribution in PMN.
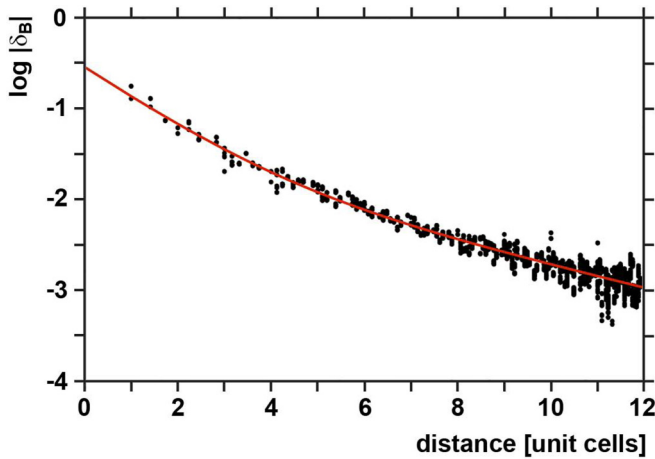
FIG. 4. Absolute value of the normalized oscillatory part of the electron density at perovskite B sites around the reference niobium ion as a function of the interatomic distance. Point symbols are data obtained from the $f(\mathbf{r})$ of Fig. 3, the continuous line is a two-exponential fit described in the text.

IV. CHEMICALLY ORDERED REGIONS

Let us briefly discuss the obtained results in the context of the concept of "chemically ordered regions" (CORs). The CORs were originally introduced in the PMN context as strictly rocksalt-ordered regions, i.e., areas with regularly alternating niobium and magnesium ions along all three [001] directions. The volume of such a region, here denoted as an α-COR, contains an equal fraction of niobium and magnesium ions. Therefore, in order to reach the overall nominal 2:1 ratio given by the stoichiometry of PMN, the α-CORs would need to be embedded in a niobium-rich *matrix*, covering at least 1/3 of the total volume. Due to the unequal valency of niobium and magnesium ions, α-CORs are charged. Therefore structural models based on these nonstoichiometric α-CORs are usually denoted as "space-charge models." Since PMN is a dielectric material, the electrostatic considerations imply that individual α-CORs can hardly be too large. It has been estimated that the largest region that can be compensated by a unit-cell thick shell of the niobium-dominated material would have a diameter of about 5 nm only [42].

An alternative picture of COR is considered in the so-called charge-balanced random site model [46]. There the chemically ordered regions are associated with a structural arrangement, in which every second nearest neighbor B site is occupied exclusively by niobium ions (B^{II}), while the intermediate sites (B^{I}) are occupied randomly by niobium and magnesium with an inverted frequency, 1:2. Therefore, the B^{I} sites (with shared occupancy) are arranged in the same regular manner as magnesium ions in an α-COR. Let us denote such a COR as a β-COR. Clearly the β-COR has the same overall composition (2:1) as the nominal chemical formula of PMN. These stoichiometric β-CORs can be thus embedded in the disordered matrix of the same composition. The overall charge balance does not impose any limitations on the volume fraction of the disordered matrix in the system, and in particular, the presence of β-COR-like order does not require the coexistence of the ordered and disordered phase at all.

Let us stress that none of the models described above defines uniquely the short-range correlations between the niobium occupancy within the neighboring B sites. The obvious reasons include the unknown correlations of the B-site occupation in the disordered matrix and in the disordered (B^{I}) sublattice of β-CORs [46], the so far unspecified size and shape distributions of CORs, the relative volume fraction of CORs, etc. Moreover, in the case of nanometer-size CORs, the two pictures are not as exclusive as it seems at first sight.

To clarify this point, let us consider a plausible distribution of B sites on a [100] plane, shown in Fig. 5(a). In the area displayed there, we have selected few compact areas aimed to become β-CORs. Within each such designed β-CORs, one checkerboard sublattice was filled by niobium and the other was filled by niobium and magnesium randomly with 2:1 frequency. The rest of the displayed area was considered as a disordered stoichiometric lattice, so that there the niobium and magnesium were distributed randomly with 1:2 frequency. While this B-site distribution was created according to the charge-balanced random site model, one can locate numerous regions with strictly rocksalt order, in particular within the originally designed β-CORs. This last circumstance can be understood because the unit cell of the α-COR is one of the structural motifs that are statistically quite likely to be present within the β-COR.

In fact, a satisfactory definition of a COR should allow us to identify the COR together with its borders uniquely in any given B-site distribution. An interesting possibility for such a definition is to postulate that *all B sites for which all its nearest neighbors are niobium ions belong to the COR*. The neighborhood of such B sites is the same as that of the B^{I} sites in the earlier described ideal structure of the β-COR. We found it reasonable to include each such B site into the COR volume together with an octahedron having corners at the six nearest neighbor B sites, i.e., with the polyhedron, that represents the fully symmetric primitive unit cell of the perfect rocksalt-ordered structure. This naturally respects the requirement that B^{I} and B^{II} sites are equally frequent in such a COR, but it obviously does not guarantee the average Nb:Mg ratio within CORs individually or altogether to be strictly 1:2. Let us call these well defined regions the γ-CORs.

The γ-COR definition is applied to the B-site distribution of Fig. 5(a), for obvious reasons considering only the four neighbors within the displayed plane. For this purpose, periodic boundary conditions are applied. The γ-CORs constructed in this way are shown in Fig. 5(b) as shaded areas. Two kinds of shading are used to distinguish the two corresponding antiphase domain states. As expected, the central area of the circular β-CORs originally designed in Fig. 5(a) belongs to the corresponding γ-CORs, but overall, the borders are largely shifted due to the randomness in the generated configuration.

Let us emphasize that γ-CORs actually include all B sites susceptible to be inner B^{I} sites of a β-COR from the point of view of the first neighbors. Whenever such a B^{I} site happens to be a magnesium ion, it can also be considered as a B^{I} site of an α-COR. Therefore, γ-COR represents a generalization of the α-COR and β-COR concepts.

In case of γ-CORs, little volume remains for the "matrix" [see Fig. 5(b)]. It is worth noting that this residual matrix contains several clusters of magnesium ions. By definition, the
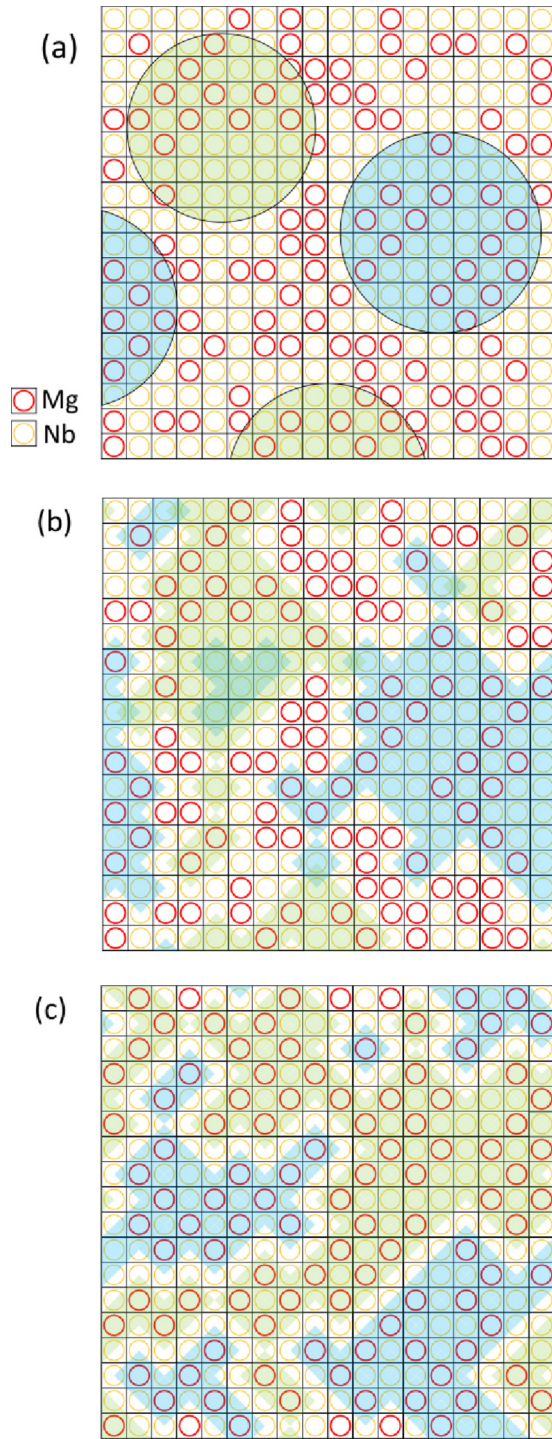
FIG. 5. Plausible distributions of niobium and magnesium ions within a (100)-oriented atomic plane. Top (a), atomic distribution with *a priori* designed β-CORs (dark-shaded areas) in a stoichiometric disordered matrix. Middle (b), identical distribution but decorated with γ-CORs, determined according to the algorithm described in the text. Bottom (c), random atomic distribution generated under requirements of stoichiometry and strict absence of magnesium ion pairs at the nearest neighbor sites. The γ-CORs are determined according to the algorithm described in the text.

nearest neighbor magnesium ions are not allowed inside any of the above defined CORs. In particular, there is no such nearest

neighbor magnesium pair within the circular areas drawn in Fig. 5(a), however, such pairs are obviously allowed to occur in the "stoichiometric matrix area" around them. Nevertheless, the "matrix area" in Fig. 5(b) contains a larger fraction of magnesium ions than 1/3 (i.e., more that than the average stoichiometric fraction), while the γ-CORs have a *smaller* Mg fraction than 1/3.

Figure 5(c) shows another B-site distribution, where exactly 1/3 of the sites are occupied by magnesium ions. These were distributed randomly, provided that the nearest neighbor magnesium ions are avoided. The shading shows subsequent assignment to the γ-CORs according to the definition given above. Here the γ-CORs have a *larger* Mg fraction than the stoichiometric one. Indeed, there are only six magnesium ions in the "residual matrix area." They are located in the top and bottom row of Fig. 5(c), because the periodic boundary conditions between the top and bottom of the image were not considered when the magnesium ions were distributed. Most interestingly, an even larger area now belongs to γ-CORs even though *a priori* no CORs were intentionally introduced in this case. The unshaded area could be considered as the antiphase boundary. In other words, in spite of the substantial randomness in the applied generating algorithm, this structure could be considered an almost fully ordered structure.

V. DISCUSSION

The above considerations indicate that obtaining comprehensive quantitative information about the B-site atom distribution in PMN is a rather delicate task. Strictly speaking, the presence of CORs as described above does not necessarily guarantee that the atomic distribution in the B sites has undergone an order-disorder phase transition.

The often cited Z-contrast imaging TEM experiments [45] clearly demonstrated the presence of large chemically ordered domains in La-doped PMN, as well as that these domains cannot have the structure of α-CORs, because the observed contrast is much smaller than that expected for α-CORs. Unfortunately, the Z-contrast data for pure PMN were not conclusive at all [42]. By analogy with the La-doped PMN case one can expect that α-CORs are not suitable for description of pure PMN either. In fact, since no well-defined CORs were directly seen in the pure PMN, it can only be inferred that CORs of the pure PMN, if present, are smaller than the TEM sample thickness (which was about 20 nm according to Ref. [42]). The hypothesis of β-like CORs with a diameter of few nanometers is well compatible with many other simple estimates based on other TEM or x-ray data (see Ref. [42] and references therein). However, in general, the available TEM and x-ray data for PMN, including the Z-contrast data showing the alternating intensities of adjacent atomic columns in Ref. [45], could be so far equally well explained by the unusually strong spatial compositional fluctuations within a chemically *disordered* state [46].

Nevertheless, taking into account the fact that the leading correlation length of the averaged short-range order observed in the present experiment is much smaller than the thickness of the TEM specimen of Ref. [45], it can be now inferred that these TEM images actually do give an evidence for some kind of chemically ordered domains. Conversely, the

averaged short-range order demonstrated here cannot be explained solely as a consequence of the size distribution of γ-like chemically ordered domains, because then such a short correlation length would be in contradiction with the observations by the Z-contrast technique. We can thus conclude that there is a very strong short-range order present in PMN, probably located both in the γ-like chemically ordered domains or in the disordered matrix area, if there is any. This short-range order, largely independent on the size of the chemically ordered domains, is likely to be of a great importance for relaxor properties of PMN.

In principle, the present experiment provides the missing information about the short-range order in PMN in a very direct manner. The main advantage of the present approach to PMN is that it gives a statistically representative information on the occupational correlations among *individual* atomic sites. For example, the present data allow us to determine probability $\rho_{[100]}^{\mathrm{MgMg}}$ of finding two magnesium ions at the nearest neighbor sites, and also the conditional probability $\mu_{[100]}$ to find a magnesium ion as the nearest neighbor of a given magnesium site. The calculation exploits the experimentally determined value of the relative scattering amplitude of the nearest neighbor of niobium ion, $f_{[100]}/\widehat{f}_{\mathrm{B}} \doteq 0.86$. This quantity can be obviously expressed through the conditional probability $\nu_{[100]}$ to find niobium ion as the nearest neighbor of a given niobium site,

$$\frac{f_{[100]}}{\widehat{f}_{\mathrm{B}}} = \frac{f_{\mathrm{Nb}}\nu_{[100]} + f_{\mathrm{Mg}}(1 - \nu_{[100]})}{f_{\mathrm{Nb}}x + f_{\mathrm{Mg}}(1 - x)}, \tag{2}$$

where f_{Nb} and f_{Mg} are atomic scattering amplitudes and $x = 2/3$ is the overall relative fraction of niobium ions. Using the tabulated values of the atomic scattering amplitudes, $f_{\mathrm{Nb}}/f_{\mathrm{Mg}} \doteq 0.324$, this equation allows us to evaluate the probability $\nu_{[100]} \doteq 0.506$. Furthermore, the nearest neighbor conditional probabilities allow us to express the nearest neighbor two-site probabilities (probabilities of distinct atomic configurations at the nearest neighbor pair of sites) as follows:

$$\rho_{[100]}^{\mathrm{NbNb}} = x\nu_{[100]}, \tag{3}$$

$$\rho_{[100]}^{\mathrm{MgNb}} = \rho_{[100]}^{\mathrm{NbMg}} = x(1 - \nu_{[100]}) = (1 - x)(1 - \mu_{[100]}), \tag{4}$$

$$\rho_{[100]}^{\mathrm{MgMg}} = (1 - x)\mu_{[100]}. \tag{5}$$

Since in a stoichiometric PMN all B sites are occupied, $\rho_{[100]}^{\mathrm{NbNb}} + \rho_{[100]}^{\mathrm{MgMg}} + \rho_{[100]}^{\mathrm{MgNb}} + \rho_{[100]}^{\mathrm{NbMg}} = 1$. The system of the

above equations then has a single solution, giving numerically $\mu_{[100]} \doteq 0.012, \rho_{[100]}^{\mathrm{MgMg}} \doteq 0.004$.

Thus, according to our experiment, there is only about 0.4% of the Mg-Mg nearest neighbor pairs present in PMN, the rest corresponds to Nb-Nb pairs (33.7%) and Mg-Nb pairs (65.8%). Similar estimates could be done for the next nearest neighbor sites or more complex correlations, but this result is of a particular significance, as it quantifies the tendency of the system to avoid the Mg-Mg pairs at the nearest neighbor B-site positions. This result thus gives a firm basis for the understanding of how strong the short-range tendency to the 1:1 B-site order actually is in PMN. It can be deduced that it is caused by the sizable strength of the nearest neighbor interactions. Obviously these strong short-range interactions are frustrated by long-range interactions, preventing thus the formation of large α-CORs.

VI. CONCLUSIONS

In summary, the present work gives evidence for sub-nanometric correlation length and isotropic nature of the Nb/Mg distribution in the model relaxor system PMN. These conclusions were drawn from the image of the average electron density distribution around the niobium ion. The image was directly reconstructed from the measured distribution of the anomalous portion of the resonant x-ray scattering intensity in the reciprocal space, involving both a discrete and continuous part (the Bragg reflections and diffuse scattering). The diameter of the entire imaged region was about 10 nm but it could be even further increased by improvement of the momentum space resolution of the experiment. These results are very interesting for understanding the physics of PMN and related relaxor ferroelectrics, but they also nicely demonstrate that this direct (model-free) method can be indeed used for three-dimensional imaging of short-range correlations with an atomic resolution and within the diameter of about 10 nm. We believe that the method could be of interest in many other areas of the current condensed matter physics and material science research.

[1] H. A. Hauptman, Rep. Prog. Phys. **54**, 1427 (1991).

[2] C. Giacovazzo, H. L. Monaco, G. Artioli, D. Viterbo, G. Ferraris, G. Gilli, G. Zanotti, and M. Catti, *Fundamentals of Crystallography. International Union of Crystallography Texts on Crystallography Texts on Crystallography*, International Union of Crystallography (Oxford University Press, Oxford, 1992).

[3] D. J. Als-Nielsen and D. McMorrow, *Elements of Modern X-ray Physics* (Wiley, New York, 2001).

[4] A. L. Patterson, Z. Kristallogr. **90**, 517 (1935).

[5] M. Buerger, *Vector Space and Its Application in Crystal-Structure Investigation* (Wiley, New York, 1953).

[6] V. Petricek, M. Dusek, and L. Palatinus, Z. Kristallogr. **229**, 345 (2014).

[7] G. M. Sheldrick, Acta Crystallogr. Sect. A **46**, 467 (1990).

[8] L. Palatinus and G. Chapuis, J. Appl. Crystallogr. **40**, 786 (2007).

[9] T. R. Welberry, *Diffuse X-ray Scattering and Models of Disorder* (Oxford University Press, Oxford, 2004).

[10] A. Guinier, *X-ray Diffraction* (W. H. Freeman & Co., San Francisco, 1963).

[11] W. A. Hendrickson and M. M. Teeter, Nature (London) **290**, 107 (1981).

[12] D. E. Sayers, E. A. Stern, and F. W. Lytle, Phys. Rev. Lett. **27**, 1204 (1971).

[13] J. J. Rehr and R. C. Albers, Rev. Mod. Phys. **72**, 621 (2000).

[14] M. Tegze and G. Faigel, Nature (London) **380**, 49 (1996).

[15] A. Szöke, AIP Conf. Proc. **147**, 361 (1986).

[16] M. Kopecký, J. Appl. Crystallogr. **37**, 711 (2004).

[17] M. Kopecký, J. Fábry, J. Kub, A. Lausi, and E. Busetto, Phys. Rev. Lett. **100**, 195504 (2008).

[18] L. E. Cross, Ferroelectrics **76**, 241 (1987).

[19] G. A. Smolenskii, V. A. Isupov, A. I. Agranovskaya, and S. N. Popov, Fiz. Tverd. Tela (Leningrad) **2**, 2906 (1960) [Sov. Phys. Solid State **2**, 2584 (1961)].

[20] V. Westphal, W. Kleemann, and M. D. Glinchuk, Phys. Rev. Lett. **68**, 847 (1992).

[21] G. A. Smolenskii and A. I. Agranovskaia, Sov. Phys. Tech. Phys. **3**, 1380 (1958).

[22] R. Blinc, *Advanced Ferroelectricity* (Oxford University Press, New York, 2011).

[23] Z.-G. Ye, Key Eng. Mater. **155-156**, 81 (1998).

[24] R. A. Cowley, S. N. Gvasaliya, S. G. Lushnikov, B. Roessli, and G. M. Rotaru, Adv. Phys. **60**, 229 (2011).

[25] W. Hu, K. Hayashi, K. Ohwada, J. Chen, N. Happo, S. Hosokawa, M. Takahasi, A. A. Bokov, and Z.-G. Ye, Phys. Rev. B **89**, 140103 (2014).

[26] V. Bovtun, S. Kamba, A. Pashkin, M. Savinov, P. Samoukhina, J. Petzelt, I. P. Bykov, and M. D. Glinchuk, Ferroelectrics **298**, 23 (2004).

[27] R. Pirc and R. Blinc, Phys. Rev. B **76**, 020101(R) (2007).

[28] A. E. Glazounov and A. K. Tagantsev, Appl. Phys. Lett. **73**, 856 (1998).

[29] D. Viehland, S. J. Jang, L. E. Cross, and M. Wuttig, J. Appl. Phys. **68**, 2916 (1990).

[30] D. Phelan, C. Stock, J. A. Rodriguez-Rivera, S. Chi, J. Leao, X. Long, Y. Xie, A. A. Bokov, Z.-G. Ye, P. Ganesh, and P. M. Gehring, Proc. Nat. Acad. Sci. USA **111**, 1754 (2014).

[31] D. Viehland and J.-F. Li, J. Appl. Phys. **74**, 4121 (1993).

[32] L. A. Bursill, H. Qian, J. L. Peng, and X. D. Fan, Physica B **216**, 1 (1995).

[33] H. Takenaka, I. Grinberg, and A. M. Rappe, Phys. Rev. Lett. **110**, 147602 (2013).

[34] M. Pasciak, T. R. Welberry, J. Kulda, M. Kempa, and J. Hlinka, Phys. Rev. B **85**, 224109 (2012).

[35] S. Tinte, B. P. Burton, E. Cockayne, and U. V. Waghmare, Phys. Rev. Lett. **97**, 137601 (2006).

[36] P. Ganesh, E. Cockayne, M. Ahart, R. E. Cohen, B. Burton, R. J. Hemley, Y. Ren, W. Yang, and Z.-G. Ye, Phys. Rev. B **81**, 144102 (2010).

[37] A. Al-Barakaty, S. Prosandeev, D. Wang, B. Dkhil, and L. Bellaiche, Phys. Rev. B **91**, 214117 (2015).

[38] A. R. Akbarzadeh, S. Prosandeev, E. J. Walter, A. Al-Barakaty, and L. Bellaiche, Phys. Rev. Lett. **108**, 257601 (2012).

[39] I. Grinberg, Y.-H. Shin, and A. M. Rappe, Phys. Rev. Lett. **103**, 197601 (2009).

[40] M. Sepliarsky and R. E. Cohen, J. Phys. Condens. Matter **23**, 435902 (2011).

[41] Q. Zhang, H. You, M. L. Mulvihill, and S. Jang, Solid State Commun. **97**, 693 (1996).

[42] D. M. Fanning, I. K. Robinson, S. T. Jung, E. V. Colla, D. D. Viehland, and D. A. Payne, J. Appl. Phys. **87**, 840 (2000).

[43] A. Tkachuk and H. Chen, arXiv:cond-mat/0303012.

[44] S. B. Vakhrushev, A. Naberezhnov, S. K. Sinha, Y.-P. Feng, and T. Egami, J. Phys. Chem. Solids **57**, 1517 (1996).

[45] Y. Yan, S. J. Pennycook, Z. Xu, and D. Viehland, Appl. Phys. Lett. **72**, 3145 (1998).

[46] P. K. Davies and M. A. Akbas, J. Phys. Chem. Solids **61**, 159 (2000).

[47] A. D. Hilton, D. J. Barber, C. A. Randall, and T. R. Shourt, J. Mat. Sci. **25**, 3461 (1990).

[48] J. Chen, H. M. Chan, and M. P. Harmer, J. Am. Ceram. Soc. **72**, 593 (1989).

[49] C. Boulesteix, V. Varnier, A. Llebaria, and E. Husson, J. Solid State Chem. **108**, 141 (1994).

[50] T.-F. Tsai, M.-H. Lin, R.-Y. Yang, and H.-Y. Lu, Mat. Sci. Eng. A **372**, 56 (2004).

[51] H. Z. Jin, J. Zhu, S. Miao, X. W. Zhang, and Z. Y. Cheng, J. Appl. Phys. **89**, 5048 (2001).

[52] A. Al-Zein, J. Hlinka, J. Rouquette, and B. Hehlen, Phys. Rev. Lett. **105**, 017601 (2010).

[53] B. Hehlen, G. Simon, and J. Hlinka, Phys. Rev. B **75**, 052104 (2007).

[54] A. Bosak, D. Chernyshov, S. Vakhrushev, and M. Krisch, Acta Crystallogr. Sect. A **68**, 117 (2012).

[55] I.-K. Jeong, T. W. Darling, J. K. Lee, Th. Proffen, R. H. Heffner, J. S. Park, K. S. Hong, W. Dmowski, and T. Egami, Phys. Rev. Lett. **94**, 147602 (2005).

[56] H. You and Q. M. Zhang, Phys. Rev. Lett. **79**, 3950 (1997).

[57] M. Pasciak and T. R. Welberry, Z. Kristallogr. **226**, 113 (2011).

[58] P. M. Gehring, H. Hiraka, C. Stock, S.-H. Lee, W. Chen, Z.-G. Ye, S. B. Vakhrushev, and Z. Chowdhuri, Phys. Rev. B **79**, 224109 (2009).

[59] G. Xu, Z. Zhong, Y. Bing, Z.-G. Ye, and G. Shirane, Nat. Mater. **5**, 134 (2006).

[60] M. Pasciak, M. Wolcyrz, and A. Pietraszko, Phys. Rev. B **76**, 014117 (2007).

[61] S. Vakhrushev, A. Ivanov, and J. Kulda, Phys. Chem. Chem. Phys. **7**, 2340 (2005).

[62] G. Burns and F. H. Dacol, Solid State Commun. **48**, 853 (1983).

[63] B. P. Burton, J. Phys. Chem. Solids **61**, 327 (2000).

[64] B. E. Warren, *X-ray Diffraction* (Dover, New York, 1969).